

# A novel polymer microneedle fabrication process for active fluidic delivery

Bernardo Cordovez · Aram J. Chung ·  
Michael Mak · David Erickson

Received: 12 July 2010 / Accepted: 9 September 2010 / Published online: 12 October 2010  
© Springer-Verlag 2010

**Abstract** In this article, we explore a new fabrication process for a flexible, all polymer, active fluidic delivery system, incorporating a fusion of laser micromachining and microfabrication techniques as well as rapid prototyping technology. Here, we show selective fluidic delivery from isolated microchannels through an electrochemically driven pumping reaction, demonstrate the dispensing of dose volumes up to 5.5  $\mu\text{l}$ , and evaluate the device's performance in terms of its delivery speed and ejection efficiency. Finally, we move this work toward an implantable microfluidic drug delivery device by investigating the device's biocompatibility through a statistical approach that overviews the viability of bovine aortic endothelial cells on polyimide and silicon substrates.

**Keywords** Implantable drug delivery · Microfluidics · Polyimide · Rapid prototyping · Electrochemistry

## 1 Introduction

Advancements in implantable drug delivery systems have enabled the transition from passive delivery to active schemes. While passives technologies (Ahmed et al. 2002;

Grayson et al. 2005; Ainslie and Desai 2008; Ainslie et al. 2009) are characterized by immediate drug release upon insertion or ingestion and are generally driven by diffusive transport, active control (Prescott et al. 2006; Santini et al. 1999; Chung et al. 2008, 2009; Chung and Erickson 2009) provides the ability to localize drug delivery with microscopic precision, direct the timing of release, and control the rate of release. These systems have been used in applications ranging from potential medical uses including hemorrhagic shock prevention through rapid vasopressin delivery (Chung and Erickson 2009), polypeptide delivery for therapeutics (Prescott et al. 2006), controlled anti epileptic drug release (Huang et al. 2009), angiogenesis control (Cao and Langer 2010), to on command chemically induced paralysis of live micro-air vehicles (Chung et al. 2009).

Polymer micro-needles are of interest for implantable drug delivery due to their enhanced biocompatibility (Richardson et al. 1993), and capability to conform to tissue without shattering during the insertion or tissue reconfiguration processes (Aoyagi et al. 2008). These devices have been fabricated using several polymers including polydimethylsiloxane (PDMS) (Tsai et al. 2009; Chen et al. 2009), polylactic and polyglycolic acid (PLGA) (Aoyagi et al. 2008; Park et al. 2005), block copolymer hydrogels (Morishita et al. 2006), SU-8 photoresist (Ane et al. 2010), and polyimide (Metz et al. 2004; Ichimori et al. 2006). Among these, polyimide is particularly useful due to its electrical and thermal insulation properties as well as its capability to be patterned directly through microfabrication. To date, however, most polymer-based drug delivery devices have either relied upon passive schemes as discussed above, or employ complicated and not easily integratable active delivery methods like peristaltic pumping through piezo-electrics (Aoyagi et al.

---

**Electronic supplementary material** The online version of this article (doi:10.1007/s10404-010-0709-x) contains supplementary material, which is available to authorized users.

---

B. Cordovez · A. J. Chung · D. Erickson (✉)  
Sibley School of Mechanical and Aerospace Engineering,  
Cornell University, 240 Upson Hall, Ithaca, NY 14853, USA  
e-mail: de54@cornell.edu

M. Mak  
Department of Biomedical Engineering, Cornell University,  
Ithaca, NY, USA

2008), large peristaltic pumps (Chen et al. 2009), and syringe pumps (Metz et al. 2004; Ichimori et al. 2006).

In this article, we present a device that incorporates the flexibility and biocompatibility of polymer microneedles while still offering the advantages of active fluidic delivery devices in a simple microfluidic architecture. Our device uses a similar electrochemical release and dose control mechanism as our previous work (Chung and Erickson 2009) but is now integrated into a flexible system as opposed to its silicon predecessor. In this article, we present our fabrication methodology and electrochemical ejection performance. Furthermore, we illustrate the device's ability to selectively dispense from different electrochemical chambers and also provide an assessment of the system's enhanced biocompatibility by analyzing the viability of bovine aortic endothelial cells on our polyimide surfaces in comparison with silicon substrates.

## 2 Flexible electrochemical-based fluidic delivery

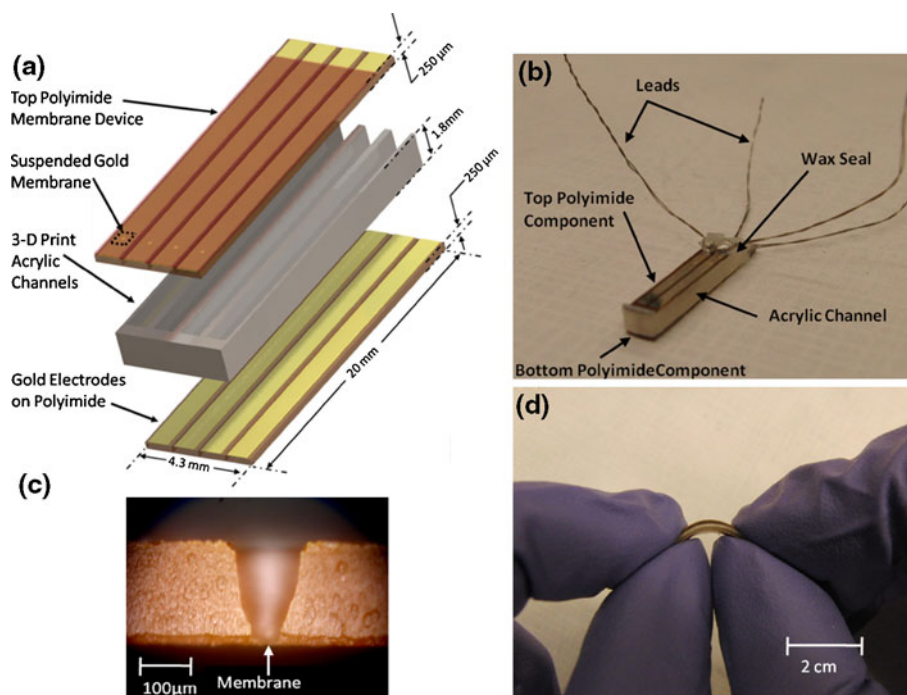
### 2.1 Device layout and operation

Figure 1a illustrates the device constituents and assembly procedure. Briefly, the device assembly consists of a top 250  $\mu\text{m}$  thick double sided polished polyimide substrate which hosts a gold electrode and a 400  $\mu\text{m}^2$  suspended gold membrane. The fluid contents are stored in 3D printed acrylic channels which can store up to 15  $\mu\text{l}$  of solution,

and the system is closed by a bottom polyimide component which contains a counter gold electrode. For more information on the component fabrication and assembly, please see Supplementary Figs. 2 and 3. As will be detailed in the next paragraph, the fluidic contents will burst through the gold membrane and into the chip's exterior through an electrochemical reaction generated by applying an electric potential between the top and bottom electrodes. Figure 1b shows a fully assembled two-channel flexible microfluidic needle. A cross-section image of the top polyimide device fabrication procedure after the laser etching, dry etching, and chrome wet etch steps which result in suspended gold membranes roughly 400  $\mu\text{m}^2$  in size is presented in Fig. 1c. Unlike our previous silicon-based devices (Chung and Erickson 2009; Chung et al. 2009), our new architecture is fully flexible as presented in Fig. 1d, and has the ability to adapt to tissue effectively for localized delivery. For more details on the fabrication procedure, please refer to Sect. 3 and Supplementary Figs. S1 and S2. Furthermore, the new flexible version can contain up to four individually addressable fluidic channels which contain the same amount of payload in each channel as its previous single chamber silicon counterpart for the same device geometry.

Figure 2 shows a time-lapse of images of the electrochemical ejection procedure, and its corresponding movie file can be found in Online Resource 1. The basic electrochemical pumping operation procedure was established in our previous publication (Chung and Erickson 2009) and by Santini et al. (1999), but briefly the drug delivery system

**Fig. 1** Device layout and assembly. **a** Schematic of the device subcomponents and assembly procedure. **b** A two channel flexible electrochemical needle. **c** Cross-section of the top polyimide device fabrication procedure after the laser etching, dry etching, and chrome wet etch steps. **d** Device in bending

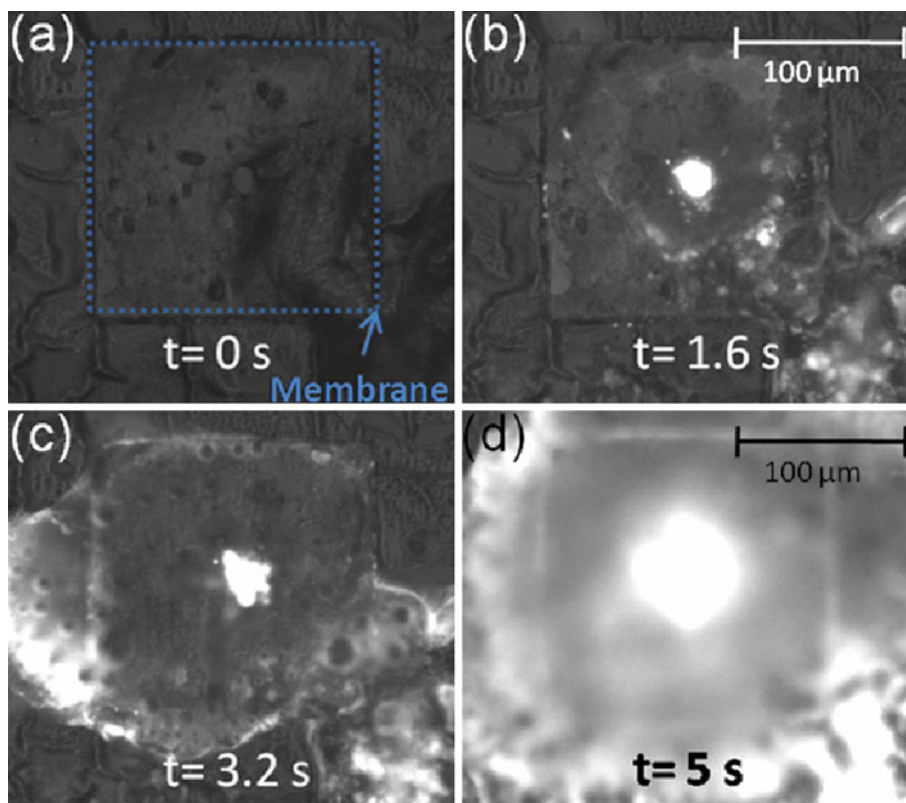


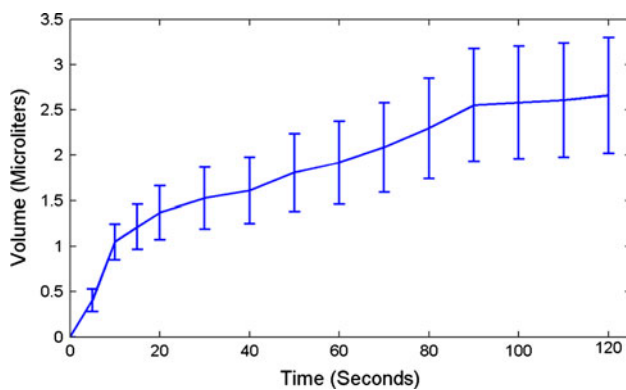
works by a two phase electrochemical reaction driven between the capping gold membrane and the bottom electrode located inside the reservoir. First, the electrolytic component of the reaction builds up the pressure in the closed fluidic system due to electrolysis (i.e. as gas bubbles are formed in the closed channel, the pressure in the chamber builds up). In addition, at the anode, chlorine ions in the buffer solution react with the gold membrane to form a water soluble chlorogold complex that degrades as the reaction proceeds (Frankenthal and Siconolfi 1982) until it ruptures and opens as demonstrated. Finally, the pressure is relieved by ejecting the fluidic contents to the chip's exterior. After applying a 30 V potential for 40 s, gold dissolution occurring in the state that we note as  $t = 0$  (Fig. 2a). The fluidic ejection procedure 1.6 and 3.2 s later is shown in Fig. 2b, c, respectively, in which the PBS solution containing 50 nm fluorescent polystyrene microspheres. The ejection flow rate rapidly increases from  $t = 5$  s (Fig. 2d) onwards, dispensing nearly 3  $\mu\text{l}$  of solution out of the well in over the course of 2 min. Right after the onset of rupture, the ejection procedure becomes more rapid as the membrane aperture size increases. Though usually uniform, we did notice that fluid ejection to the outside environment can occur in spurts.

Figure 3 displays the mean ejection volume as a function of time for experiments operated at a 30 V potential.

The ejection volumes were measured by placing a cover-slip at a measured distance above the membrane, and relating the wetted area (measured using image software Image J) to ejection volume using a simple flat cylinder model. The high applied electrical potential was chosen here since it was previously found that the fluid ejection rate increases with the magnitude of the electric potential (Chung et al. 2008; Chung and Erickson 2009). For these conditions, on average 17% of the contents managed to eject out of the system after 2 min. In most experiments, the delivery rate is highest for the first 30 s following rupture (dispensing at  $\sim 0.1 \mu\text{l/s}$ ) and decays with time. Though the general trend agrees with our previous publications (Chung et al. 2008; Chung and Erickson 2009) in the best of cases only 37% of the fluids (5.5  $\mu\text{l}$ ) managed to leave the polyimide devices, less than its previous silicon counterpart. After the main fluidic ejection, which occurs in the first 90 s of the trial, both diffusion and displacement of liquids through electrolysis are important. Because of diffusion, the device cannot fully stop dose delivery on command, however, the delivery rate is much slower. In some cases, it was found that after a certain amount of time the bubbles generated during electrolysis could get sufficiently large so as to block the main fluidic channel (acrylic) and the inverted channel (polyimide) that leads to the suspended membrane. These bubbles served to

**Fig. 2** Electrochemical ejection procedure. **a** Prior to membrane rupture and 40 s after first applying electric potential. **b** Fluidic ejection 1.6 s and **c** 3.2 s after the onset of gold membrane rupture. **d** Increased flow rate 5 s after membrane rupture





**Fig. 3** Device ejection volume performance results at 30 V

disconnect the liquid stream and generate an adverse pressure gradient, keeping some of the liquid contents from leaving the chip. In our next generation of needles, the laser micromachining etch area will be wider in order to increase the membrane aperture and enable a higher rate of delivery, and the use of gas permeable materials will be investigated to mitigate the clogging behavior. We are also looking into making a wider exposed area in the backside of the cathode than the cathode area just beneath the membrane in order to induce water electrolysis and  $H_2$  gas formation mainly in the back of the channel while still ionizing chloride ions in the vicinity of the gold solution effectively, potentially minimizing the amount of air bubbles pushed into the inverted channel. It should be noted that the mean current during ejection was 0.2 mA, thus the system consumes an average power of 6 mW, which is still very low compared to traditional autonomous delivery devices (Zahn et al. 2004; Schomburg and Menz 1995; Jang et al. 2000).

## 2.2 Multiplexing and fluidic channel addressing

Figure 4 displays a multi-chamber device with independent multiplexing capability. Figure 4a shows the selective fluidic actuation of the bottom channel in a two needle setup 41 s after ejection, and Fig. 4b shows the ability to

actuate the top channel (123 s later), with little to no cross talk between the channels. There is only a potential applied to the top channel in Fig. 4b, and the smaller ejection volume evidenced in the bottom channel is due to fluid evaporation and creeping back into the reservoir. We did observe fluidic cross talk when liquid surfaces from different channels coalesce; or after 4 min (roughly) after the electrolytic reaction starts to dissolve the epoxy adhesive that binds the polyimide substrates to the acrylic, making underflow leakage possible. This problem can be reduced by using wider acrylic channels since it will take longer to dissolve the majority of the biocompatible epoxy.

## 2.3 Biocompatibility of polyimide and silicon needles: a comparison

In Sect. 2.1, we demonstrated the high degree of flexibility of all polymer needle device and we now investigate whether polyimide it is at least as biocompatible as silicon; which is the most common substrate for current implantable micro-devices (Santini et al. 1999) and our previous material of choice (Chung and Erickson 2009). In this section, we analyze the biocompatibility of our devices using bovine aortic endothelial cells as our control biology. For more details on the cell seeding procedure, please refer to the Sect. 3. For each substrate (polyimide and silicon), cells were seeded onto the surface and submerged inside a petridish filled with cell culture media. On each of the specified days, living cells that were adherent to the substrate surface and were imaged on an upright microscope, counted, and averaged over 10 different regions, as shown in Fig. 5. Cells on the petridish surface containing one of those substrates were also counted and averaged on day 7. The areas of all regions used were the same. The average concentration on each substrate on days 2, 4, and 7 was normalized by the average concentration of cells on the petridish on day 7, and the results are shown in Fig. 6a. The initial concentration (on day 2) on the silicon substrate was higher than that on polyimide, but in the course of 1 week,

**Fig. 4** Fluidic channel multiplexing. **a** Bottom channel actuation 41 s after ejection. **b** Top channel addressing 123 s after the onset of rupture

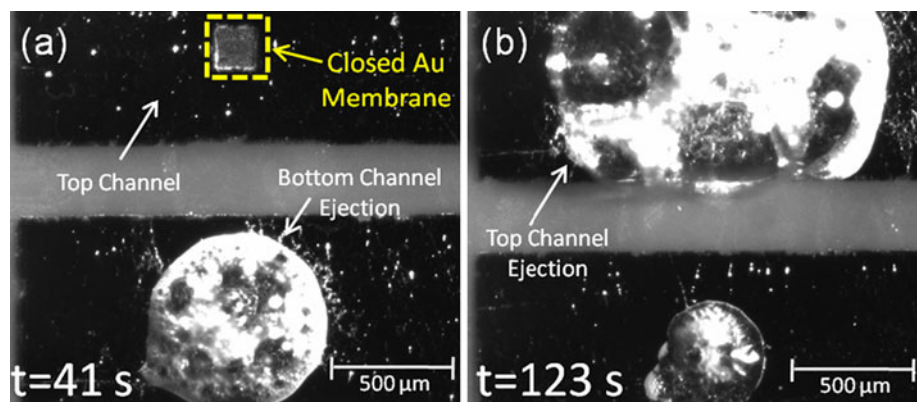


**Fig. 5** Cell viability as a function of substrate and time: viability analysis of bovine aortic endothelial cells in polyimide and silicon substrates in Days 2, 4, and 7

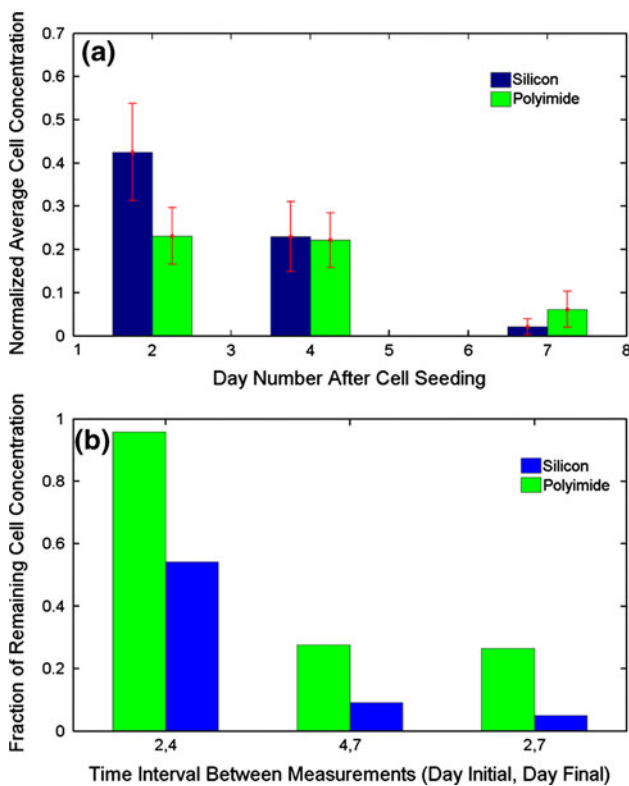
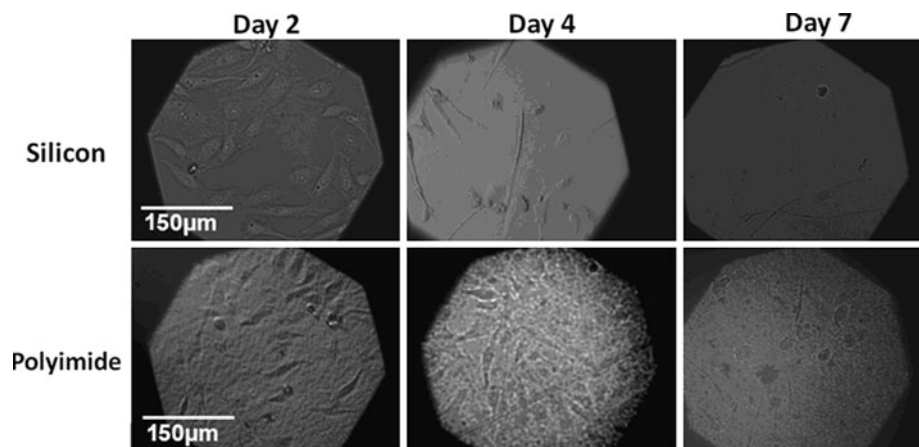


**Fig. 6** Biocompatibility of polyimide and silicon needles: **a** Normalized average cell concentration on each substrate on days 2, 4, and 7. **b** Fractional decrease in cell concentration between reference days

cell viability decreased for both, and the rate of decrease appears higher for silicon. A similar fraction of cells were found on both substrates on day 4, and very few cells survive for over 1 week as evidenced by Fig. 6b. The cell viability is comparable for silicon and polyimide, but notice particularly that the fraction of remaining cells is much higher for polyimide, and thus is likely to be a better substrate for implantation.

### 3 Fabrication and methods

#### 3.1 Top substrate fabrication

The substrate used is a double side polished, 250 µm thick polyimide substrate. The top was patterned through gold liftoff via a chrome adhesion layer that also serves as an etch stop, and an aluminum etch mask at the bottom which define the blind hole laser etch locations. The majority of the backside etch (~240 µm) was performed through a deep laser etch, which yielded a mean etch angle of 10° with the vertical. Due to heating during this etching procedure, this step was hard to control and is resulted in irregular final membrane dimensions varying from 125 to 650 µm<sup>2</sup>. The dry etching step was finished using a 70% O<sub>2</sub>, 30% CF<sub>4</sub> etch 250 W RIE power, with the role of CF<sub>4</sub> being that of etching inorganics found in the polyimide (Popova et al. 1996), enabling a quicker etch. The aluminum mask layer was removed via a wet etch. At this point, the top of the gold layer was insulated with the exception of the membrane location using a 2 µm thick photoactive polyimide, to minimize electrical interaction with the surroundings. We then wet etched the remaining chrome layer, yielding roughly a 400 µm<sup>2</sup> (on average) suspended gold membrane. The backside of this polyimide channel was then subjected to an oxygen plasma clean to ensure wettability of the substrate.

#### 3.2 Acrylic channel fabrication and softening

Channels holding ~15 µl of solution (2 mm tall and 750 µm wide), were fabricated by 3D printing of acrylic. The defined structures were then left in 2% NaOH for 60 h, which served to remove any sacrificial material remaining from the printing procedure, as well as permeate through the porous acrylic channels, making the resulting structure flexible. To make the structure water impermeable, we

deposited 2  $\mu\text{m}$  of parylene conformally around the channels.

### 3.3 Bottom electrode substrate

The bottom gold electrode was also defined on a 250  $\mu\text{m}$  thick polyimide substrate through liftoff and also uses a chrome adhesion layer. Single electrodes were diced using a laser cutter (or alternatively a scalpel). As on the top electrode, platinum contacts were placed in electrical contact with the gold through silver conductive epoxy.

### 3.4 Needle assembly and fluidic loading

After plasma treating the bottom of the top substrate to ensure that liquid fills the etched cavity that leads to the suspended gold electrode, the acrylic channels were bonded to the top and bottom polyimide by dipping the acrylic channels on a pre-spun glass slide containing Loctite 405<sup>®</sup> adhesive. The polyimide and acrylic pieces were then aligned and left to bond for 24 h. The defined channel structure was then subjected to O<sub>2</sub> plasma cleaning and the channels were then filled with a 10 mM PBS solution from the back using a microsyringe. Subsequently, the needles were shaken manually to ensure wetting of the suspended gold membrane and the release of potentially entrapped bubbles, followed by the closing of the channel structure by sealing the back with 5 min quick dry epoxy.

### 3.5 Cell culture and biocompatibility experiment setup

Bovine aortic endothelial cells were used for these experiments. They were fed with Leibovitz L-15 media and incubated at 37°C and 0% CO<sub>2</sub>. Media were replenished every day. For the experiment, one strip of silicon and one polyimide device were used as substrates for a viability comparison assay. Prior to usage, each strip was sterilized with 70% isopropanol 30% water and dried off completely. Each was placed in the bottom of separate petridishes and submerged in 2 ml of Leibovitz L-15 media, and 350 cells/mm<sup>2</sup>, suspended through trypsinization, were then seeded in each petridish. The images shown in Fig. 5 were recorded on days 2, 4, and 7 after initial cell seeding, and the petridish cell seeding of day 7 (control) is shown in Supplementary Fig. S4.

## 4 Discussion and conclusions

Though effective fluid ejection was consistently demonstrated here, in some cases the ejection rate tended to be irregular. This ejection irregularity is likely due to gas

bubbles generated through the electrolytic procedure that clogging the main fluidic channel (acrylic) and the inverted channel (polyimide) that leads to the suspended membrane. We believe that this effect also plays an important role on the overall device performance; since large gas pockets can disconnect the liquid stream and in turn generate an adverse pressure gradient, hindering the remaining fluid from leaving the chip's interior. Furthermore, since the inverted polyimide channel that leads to the membrane is narrower than that of our previous silicon-based device (see Sect. 3), gas bubble induced clogging is more likely to occur compared to our previous approach. It is also important to note that when comparing the rupture initiation time to our previous results (Chung and Erickson 2009), the polyimide-based device takes roughly 25% longer to initiate ejection since our exposed membrane has a shorter span and is thus more stiff and has a smaller area for dissolution. In future devices, the laser etch area will be wider in order to enable an increase the dose delivery rate through a larger membrane aperture. Though there is degradation in performance due to gas bubble formation, it is important to note that this chip does manage to perform both controlled and highly localized delivery in a flexible and biocompatible substrate in a small and easily implantable architecture.

Another concern is the cross-section size of the device. For a single needle setup, this dimension is 1.75 mm wide by 2 mm tall (though the fluidic cross-section is actually 0.75 mm by 1.8 mm tall), which is not small enough for effective tissue adaptation. The main spatial delimiter for the size of our devices is the fluidic loading process which involves the dispensing of fluids via a microsyringe. Our main goal here was to develop a system that can incorporate different fabrication technologies for enabling an all polymer fluidic delivery system that had a volume on the order of 10  $\mu\text{l}$ . Thus, while all the fabrication steps described are compatible with miniaturization, we did not attempt to push the limits of size here. One advantage of using a 3D printed channel is that it can generate geometries not easily attainable through microfluidic molding processes. Thus, one can easily devise alignment rails to ensure quick and accurate assembly from different subcomponents.

The multiplexing capability demonstrated by this chip does enable one to deliver different concentrations and types of chemicals (Santini et al. 1999). Furthermore, multiple channels also provide redundancy in the case of faulty post-insertion membranes, which could be damaged useful in overcrowded insertion regions. In terms of the cross channel leakage mentioned above, it takes approximately 4 min for the electrolytic reaction to dissolve the binding epoxy, placing an upper limit on the time for delivery. This time could be improved by using wider channels to prevent underflow leakage, though it would

come at the expense of a larger device. In terms of the device's biocompatibility, we conclude that cell viability, which is our measure of biocompatibility here, is comparable for silicon and polyimide, but particularly that the rate of decrease in cells appears higher for the silicon.

**Acknowledgments** The authors would like to thank Michael Kalontarov for helpful discussions, Prof. Hod Lipson for access to the 3-D Acrylic Printer and Dr. Mehmet Ozgur at the MEMS and Nanotechnology Exchange for the laser etch process. This work was supported by the Defense Advanced Research Projects Agency Defense Sciences Office under the Hybrid Insect MEMS “HI-MEMS” program through the Boyce Thompson Institute for Plant Research. Distribution unlimited. Portions of this work were also supported by the Office of Naval Research under grant “Autonomous Microfluidic Devices for Battlefield Health Assessment and Treatment” which has award number N000141010115. The facilities used for this research include Nanoscale Science & Technology Facility (CNF), Nanobiotechnology Center (NBTC) at Cornell University.

## References

- Ahmed A, Bonner C, Desai TA (2002) Bioadhesive microdevices with multiple reservoirs: a new platform for oral drug delivery. *J Controlled Rel* 81(3):291–306
- Ainslie KM, Desai TA (2008) Microfabricated implants for applications in therapeutic delivery, tissue engineering, and biosensing. *Lab Chip* 8(11):1864–1878
- Ainslie KM, Lowe RD, Beaudette TT, Petty L, Bachelder EM, Desai TA (2009) Microfabricated devices for enhanced bioadhesive drug delivery: attachment to and small-molecule release through a cell monolayer under flow. *Small* 5(24):2857–2863
- Ane A, Gemma G, Liset MDLP, María T, Anton G, Javier B, Rafa S, Rosa V, Fernández LJ (2010) SU-8-based microneedles for in vitro neural applications. *J Micromech Microeng* 20(6):064014
- Aoyagi S, Izumi H, Fukuda M (2008) Biodegradable polymer needle with various tip angles and consideration on insertion mechanism of mosquito's proboscis. *Sens Actuators A Phys* 143(1):20–28
- Cao YH, Langer R (2010) Optimizing the delivery of cancer drugs that block angiogenesis. *Sci Transl Med* 2(15):15–17
- Chen J, Chu M, Koulajian K, Wu X, Giacca A, Sun Y (2009) A monolithic polymeric microdevice for pH-responsive drug delivery. *Biomed Microdev* 11(6):1251–1257
- Chung AJ, Erickson D (2009) Engineering insect flight metabolics using immature stage implanted microfluidics. *Lab Chip* 9(5):669–676
- Chung AJ, Kim D, Erickson D (2008) Electrokinetic microfluidic devices for rapid, low power drug delivery in autonomous microsystems. *Lab Chip* 8(2):330–338
- Chung AJ, Huh SY, Erickson D (2009) A robust, electrochemically driven microwell drug delivery system for controlled vasopressin release. *Biomed Microdev* 11(4):861–867
- Frankenthal RP, Siconolfi DJ (1982) The anodic corrosion of gold in concentrated chloride solutions. *J Electrochem Soc* 129(6):1192–1196
- Grayson AC, Richards C, Michael J, Langer R (2005) Size and temperature effects on poly(lactic-co-glycolic acid) degradation and microreservoir device performance. *Biomaterials* 26(14):2137–2145
- Huang WC, Hu SH, Liu KH, Chen SY, Liu DM (2009) A flexible drug delivery chip for the magnetically-controlled release of anti-epileptic drugs. *J Controlled Rel* 139(3):221–228
- Ichimori S, Nishida K, Shimoda S, Sekigami T, Matsuo Y, Ichinose K, Shichiri M, Sakakida M, Araki E (2006) Development of a highly responsive needle-type glucose sensor using polyimide for a wearable artificial endocrine pancreas. *J Artif Organs* 9(2):105–113
- Jang J, Lee SS (2000) Theoretical and experimental study of MHD (magnetohydrodynamic) micropump. *Sens Actuators A Phys* 80(1):84–89
- Metz S, Bertsch A, Bertrand D, Renaud Ph (2004) Flexible polyimide probes with microelectrodes and embedded microfluidic channels for simultaneous drug delivery and multi-channel monitoring of bioelectric activity. *Biosens Bioelectron* 19(10):1309–1318
- Morishita M, Goto T, Nakamura K, Lowman AM, Takayama K, Peppas NA (2006) Novel oral insulin delivery systems based on complexation polymer hydrogels: single and multiple administration studies in type 1 and 2 diabetic rats. *J Controlled Rel* 110(3):587–594
- Park J-H, Allen MG, Prausnitz MR (2005) Biodegradable polymer microneedles: fabrication, mechanics and transdermal drug delivery. *J Controlled Rel* 104(1):51–66
- Popova K, Spassova E, Zhivkov I, Danev G (1996) Reactive ion etching of vapor phase deposited polyimide films in CF<sub>4</sub>/O<sub>2</sub>: effect on surface morphology. *Thin Solid Films* 274(1–2):31–34
- Prescott JH, Lipka S, Baldwin S, Sheppard NF, Maloney JM, Coppeta J, Yomtov B, Staples MA, Santini JT (2006) Chronic, programmed polypeptide delivery from an implanted, multireservoir microchip device. *Nat Biotechnol* 24(4):437–438
- Richardson RR Jr, Miller JA, Reichert WM (1993) Polyimides as biomaterials: preliminary biocompatibility testing. *Biomaterials* 14(8):627–635
- Santini JT, Cima MJ, Langer R (1999) A controlled-release microchip. *Nature* 397(6717):335–338
- Schomburg WK, Maas D, Bacher W, Bustgens B, Farehnberg MJ, Seidel D (1995) Assembly for micromechanics and LIGA. *J Micromech Microeng* 5(2):57
- Tsai H-KA, Moschou EA, Daunert S, Madou M, Kulinsky L (2009) Integrating biosensors and drug delivery: a step closer toward scalable responsive drug-delivery systems. *Adv Mater* 21(6):656–660
- Zahn JD, Deshmukh A, Pisano AP, Liepmann D (2004) Continuous on-chip micropumping for microneedle enhanced drug delivery. *Biomed Microdev* 6(3):183–190